UCLA
UCLA Previously Published Works

Title

FAM111A induces nuclear dysfunction in disease and viral restriction

Permalink

Journal

ISSN

Authors

Nie, Minghua
Oravcová, Martina
Jami-Alahmadi, Yasaman
et al.

Publication Date

DOI

Peer reviewed

SOURCE
DATA

TRANSPARENT
PROCESS

EMBO
reports

FAM111A induces nuclear dysfunction in disease and viral restriction

Minghua Nie[1] (iD), Martina Oravcová[1], Yasaman Jami-Alahmadi[2], James A Wohlschlegel[2] (iD), Eros Lazzerini-Denchi[3] & Michael N Boddy[1,*] (iD)

Abstract

Mutations in the nuclear trypsin-like serine protease FAM111A cause Kenny–Caffey syndrome (KCS2) with hypoparathyroidism and skeletal dysplasia or perinatally lethal osteocraniostenosis (OCS). In addition, FAM111A was identified as a restriction factor for certain host range mutants of the SV40 polyomavirus and VACV orthopoxvirus. However, because FAM111A function is poorly characterized, its roles in restricting viral replication and the etiology of KCS2 and OCS remain undefined. We find that FAM111A KCS2 and OCS patient mutants are hyperactive and cytotoxic, inducing apoptosis-like phenotypes such as disruption of nuclear structure and pore distribution, in a protease-dependent manner. Moreover, wild-type FAM111A activity causes similar nuclear phenotypes, including the loss of nuclear barrier function, when SV40 host range mutants attempt to replicate in restrictive cells. Interestingly, pan-caspase inhibitors do not block these FAM111A-induced phenotypes, implying it acts independently or upstream of caspases. In this regard, we identify nucleoporins and the associated GANP transcription/replication factor as FAM111A interactors and candidate targets. Overall, we reveal a potentially unifying mechanism through which deregulated FAM111A activity restricts viral replication and causes KCS2 and OCS.

Introduction

Family with sequence similarity 111 member A (FAM111A) was identified as an interactor of the SV40 large T antigen (LT) and a host range (HR) restriction factor that antagonizes productive infection by certain SV40 mutants (Fine *et al*, 2012). Specifically,

FAM111A depletion rescues replication center formation and gene expression defects of LT mutants lacking C-terminal sequences (Tarnita *et al*, 2019). Further analysis indicated that FAM111A executes its restrictive function during or following SV40 viral genome replication (Tarnita *et al*, 2019).

Expanding the role of FAM111A in protecting against viral challenge, it was identified along with the PCNA clamp-loading complex RFC1-5 as a restriction factor for orthopoxvirus HR mutants lacking the serine protease inhibitor SPI-1 (Panda *et al*, 2017). Early studies on rabbitpox virus (RPXV) HR mutants lacking SPI-1 suggested that restrictive human A459 cells exhibit apoptosis-like features upon infection, which required RPXV DNA synthesis (Brooks *et al*, 1995). However, a subsequent study found that the related vaccinia virus (VACV) lacking SPI-1 caused nuclear morphological changes such as chromatin condensation and membrane invagination, without the normal biochemical features of apoptosis (Shisler *et al*, 1999).

Thus, viruses with diverse life cycles, e.g., nuclear replication sites (polyomavirus) versus replication in the cytoplasm (orthopoxvirus), possess a mechanism to overcome inhibition by FAM111A. It is likely that FAM111A activity is triggered during viral replication, but how it combats viral challenge remains poorly understood (Luttge & Moyer, 2005; Panda *et al*, 2017; Tarnita *et al*, 2019). Consistent with its apparent replication-dependent role in viral restriction, FAM111A was identified in high-throughput screens as a protein enriched on nascent chromatin, i.e., replication forks (Alabert *et al*, 2014; Wessel *et al*, 2019). Exogenous FAM111A associated with replication sites via a PCNA interacting motif (Fig 1A; Alabert *et al*, 2014), whereas endogenous FAM111A was detected in nucleoli until S phase when, despite elevated expression, it appeared to become undetectable (Tarnita *et al*, 2019).

The FAM111A C-terminus contains a predicted trypsin-like serine protease domain with an as yet untested catalytic triad (Fig 1A). However, the role of vaccinia virus SPI-1 in antagonizing FAM111A is consistent with the presence of protease activity (Panda *et al*, 2017). Notably, dominant mutations in the FAM111A protease domain cause Kenny–Caffey syndrome type 2 (KCS2) and osteocraniostenosis (OCS), which present with hypoparathyroidism, short stature, and skeletal defects (Unger *et al*, 2013; Isojima *et al*, 2014;

1 Department of Molecular Medicine, The Scripps Research Institute, La Jolla, CA, USA
2 Department of Biological Chemistry, David Geffen School of Medicine, University of California, Los Angeles, CA, USA
3 Laboratory of Genome Integrity, National Cancer Institute, NIH, Bethesda, MD, USA
 *Corresponding author. Tel: +1 858 784 7042; Fax: +1 858 784 2265; E-mail: nboddy@scripps.edu
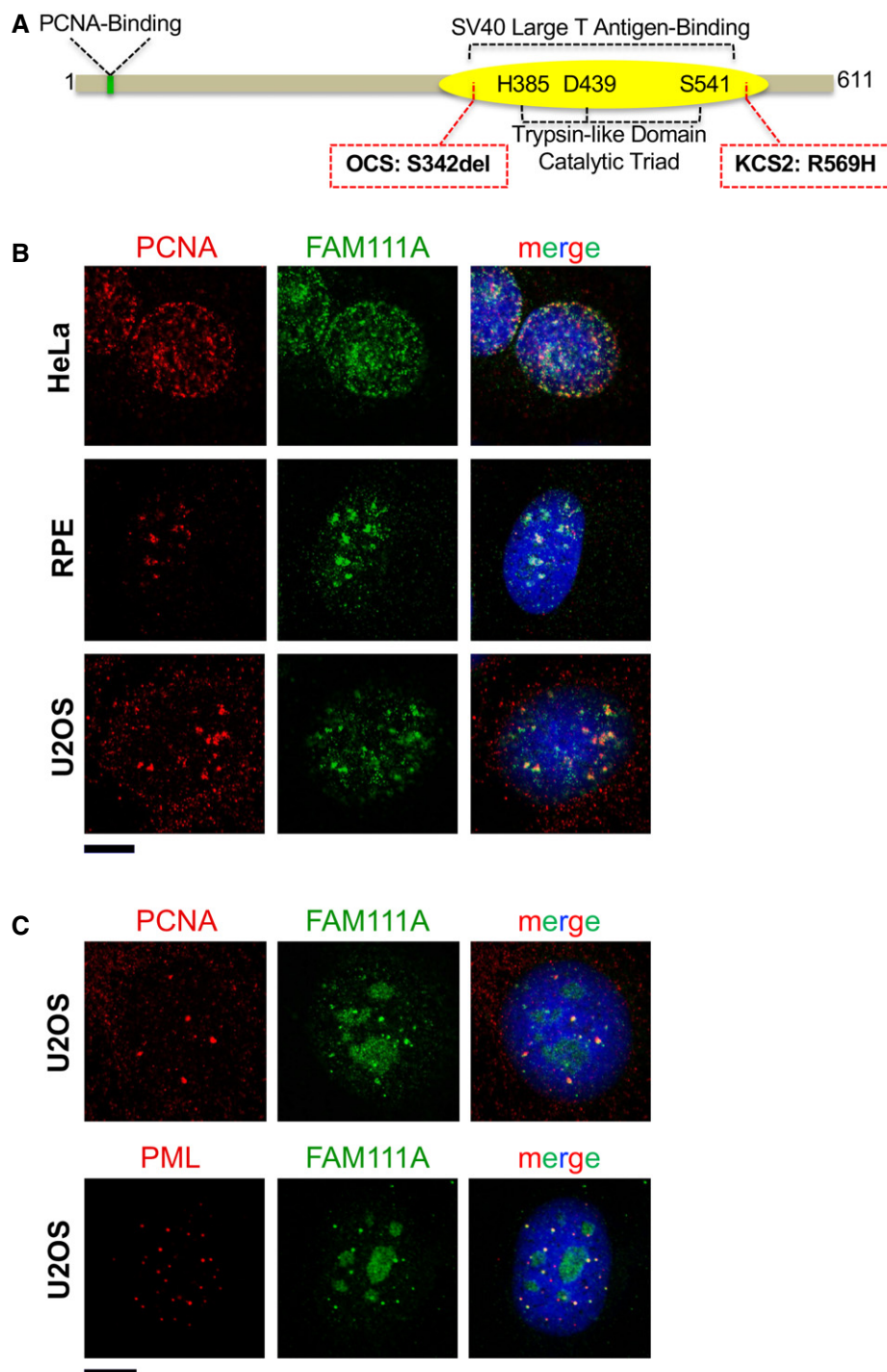
Figure 1. FAM111A localization in multiple cell lines.

A Schematic representation of human FAM111A domains and mutations that compromise FAM111A functions. The FAM111A N-terminus contains a functional PCNA interaction motif (PIP box; Alabert *et al*, 2014). The FAM111A C-terminal trypsin-like protease domain contains a typical H385-D439-S541 catalytic triad (Unger *et al*, 2013) and binds the C-terminus of the SV40 Large T antigen (Fine *et al*, 2012; Tarnita *et al*, 2019). We used an S541A mutation to disrupt the catalytic triad and inactivate FAM111A's trypsin-like protease activity. Finally, the KCS2 and OCS patient mutations are indicated in red boxes. See text and (Unger *et al*, 2013) for phenotypic details.

B Confocal microscopy images of HeLa, RPE, and U2OS cell lines that were pre-extracted with Triton X-100 before fixed with formaldehyde and costained with DAPI and antibodies against PCNA and FAM111A. Scale bar: 10 μm.

C U2OS cells were stained with antibodies against PML and FAM111A and imaged by confocal microscopy. Scale bar: 10 μm.

Source data are available online for this figure.

Nikkel *et al*, 2014). How the KCS2 and OCS mutations impact FAM111A activity remains unknown but due to their position in the protease domain, and apparent dominance over wild-type, they were suggested to be gain-of-function (Unger *et al*, 2013).

Here, we show that the FAM111A KCS2 and OCS patient mutants are more cytotoxic than wild-type FAM111A, due to deregulation of their trypsin-like protease activity. Ectopic expression of the KCS2/OCS FAM111A mutants disrupts nuclear morphology, nuclear pore distribution, DNA replication, and cell-substrate attachment in a protease activity-dependent manner. Similarly, in response to the attempted replication of polyomavirus (SV40) HR mutants in restrictive cells, endogenous FAM111A impairs nuclear barrier function, morphology, and pore distribution. Surprisingly, these phenotypes are insensitive to pan-caspase inhibitors, suggesting that FAM111A may trigger them more directly. In this regard, we identify several nuclear pore associated factors as candidate substrates of FAM111A. Overall, our data provide unifying insights into the pathological effects of KCS2/OCS FAM111A mutants, and the functions of FAM111A in viral restriction.

Results and Discussion

Endogenous FAM111A colocalizes with PCNA during replication

Earlier high-throughput studies found that FAM111A associates with nascent chromatin, but the presence of endogenous FAM111A at replication forks had not been visualized (Alabert *et al*, 2014; Wessel *et al*, 2019). Using a validated commercial FAM111A antibody in multiple cell lines, we detected the previously reported nucleolar localization (Tarnita *et al*, 2019) and also observed a focal nuclear pattern in some cells that colocalized with PCNA (Fig 1B). Based on the characteristic patterns of nuclear PCNA during DNA replication, our data confirm that FAM111A is associated with sites of replication.

Interestingly, we also detected FAM111A at distinct subnuclear foci when U2OS cells were not in S phase, as judged by the lack of nuclear PCNA staining and the predominant nucleolar localization of FAM111A (Fig 1C). Such foci were not detected in the other cell lines tested. A key difference is that U2OS cells maintain their telomeres via a recombination-based replication process called alternative lengthening of telomeres (ALT), as they do not have active telomerase (Bryan *et al*, 1997; Cesare & Reddel, 2010). ALT telomeres undergo DNA synthesis in the G2/M phases of the cell cycle at ALT-associated PML bodies (APBs) that contain PCNA among other DNA replication and repair factors (Dilley *et al*, 2016; Min *et al*, 2017; Pan *et al*, 2017; Zhang *et al*, 2019; Sobinoff & Pickett, 2020; Loe *et al*, 2020). Further analysis revealed that the atypical FAM111A foci in U2OS cells colocalize with both PCNA and PML (Fig 1C). Therefore, FAM111A localizes to sites of DNA synthesis during both bulk genome duplication and the unscheduled DNA replication/repair events at ALT telomeres.

Protease-dependent cytotoxicity of FAM111A

Genetic analysis of Kenney–Caffey syndrome 2 (KCS2) and osteocraniostenosis (OCS) revealed causative mutations in FAM111A (R569H and S342del, respectively; Fig 1A; Unger *et al*,

2013; Isojima *et al*, 2014)). Based on genetic considerations, these mutations were hypothesized to generate hyperactive variants of FAM111A (Unger *et al*, 2013). To test this, we generated a panel of inducible cell lines to study the effects of ectopically expressed wild-type and mutant FAM111A.

Ectopic expression of wild-type FAM111A strongly inhibited cell growth in HEK293 cells, whereas it had only a mild effect on U2OS cells and no significant effect on RPE cells (Fig 2A). These different responses to the ectopic expression of wild-type FAM111A may be due to the extremely low levels of endogenous FAM111A present in HEK293 versus U2OS and RPE cells (Fig EV1). We attribute the growth inhibition by FAM111A to its protease activity, since the absence of toxicity of the protease-dead mutant FAM111A^{S541A} rules out any negative effects of it competing with other proteins for PCNA binding (Fig 2A). Notably, the KCS2 (FAM111A^{R569H}) and OCS (FAM111A^{S342del}) mutants were more potent inhibitors of cell growth than wild-type FAM111A, strongly impacting all three cell lines (Fig 2A). These results are consistent with the gain-of-function hypothesis for FAM111A in KCS2 and OCS (Unger *et al*, 2013).

Paralleling its cytotoxicity, the ectopic expression of FAM111A but not protease-dead FAM111A^{S541A} also perturbed cell cycle profiles (Fig 2B, FACS -Dox in Fig EV2). In particular, FAM111A^{R569H} and FAM111A^{S342del} expression caused cells to accumulate in S phase (Fig 2B). Given the localization of FAM111A to replication forks and its protease-dependent toxicity, these results suggest that the KCS2 and OCS patient mutants disrupt replication, conceivably through the unscheduled removal of replication factors.

Ablating the protease activity of FAM111A^{R569H} and FAM111A^{S342del} with the S541A mutation mitigated both their toxicity (Fig 2C) and effects on cell cycle distribution (Fig 2D). Moreover, HEK293T cells that constitutively express the SV40 large T antigen were relatively more resistant to wild-type, FAM111A^{R569H} or FAM111A^{S342del} overexpression than HEK293 cells (Fig EV3). This supports the suspected role of the SV40 Large T antigen in inactivating FAM111A protease activity (Tarnita *et al*, 2019).

Caspase-independent cytotoxicity of FAM111A hyperactivity

Considering the foregoing, we tested whether hyperactive FAM111A induces apoptosis. Cleavage of PARP is a well-characterized marker of caspase-dependent apoptosis (Soldani & Scovassi, 2002) and was weakly detected in cells expressing wild-type FAM111A but not protease-dead FAM111A^{S541A} (Fig 3A). Notably, PARP cleavage was stronger in cells expressing FAM111A^{R569H} or FAM111A^{S342del}, despite their relatively low levels (Fig 3A). Further, the levels of ectopically expressed FAM111A were similar to those of endogenous FAM111A in HEK293 but much lower than those in U2OS cells, making their toxicity all the more striking (Fig 3A). These different ectopic/endogenous ratios of FAM111A expression may explain the higher sensitivity of HEK293 versus U2OS cells to ectopic FAM111A expression (Fig 2A).

We next tested the contribution of apoptotic induction to the profound cytotoxic effects of FAM111A^{R569H}. To this end, we used the well-characterized pan-caspase inhibitor Z-VAD-FMK to reduce apoptotic signaling in cells expressing FAM111A, FAM111A^{R569H}, FAM111A^{S541A}, or FAM111A^{S541A,R569H}. As anticipated, PARP cleavage was enhanced by FAM111A^{R569H} expression, but was largely
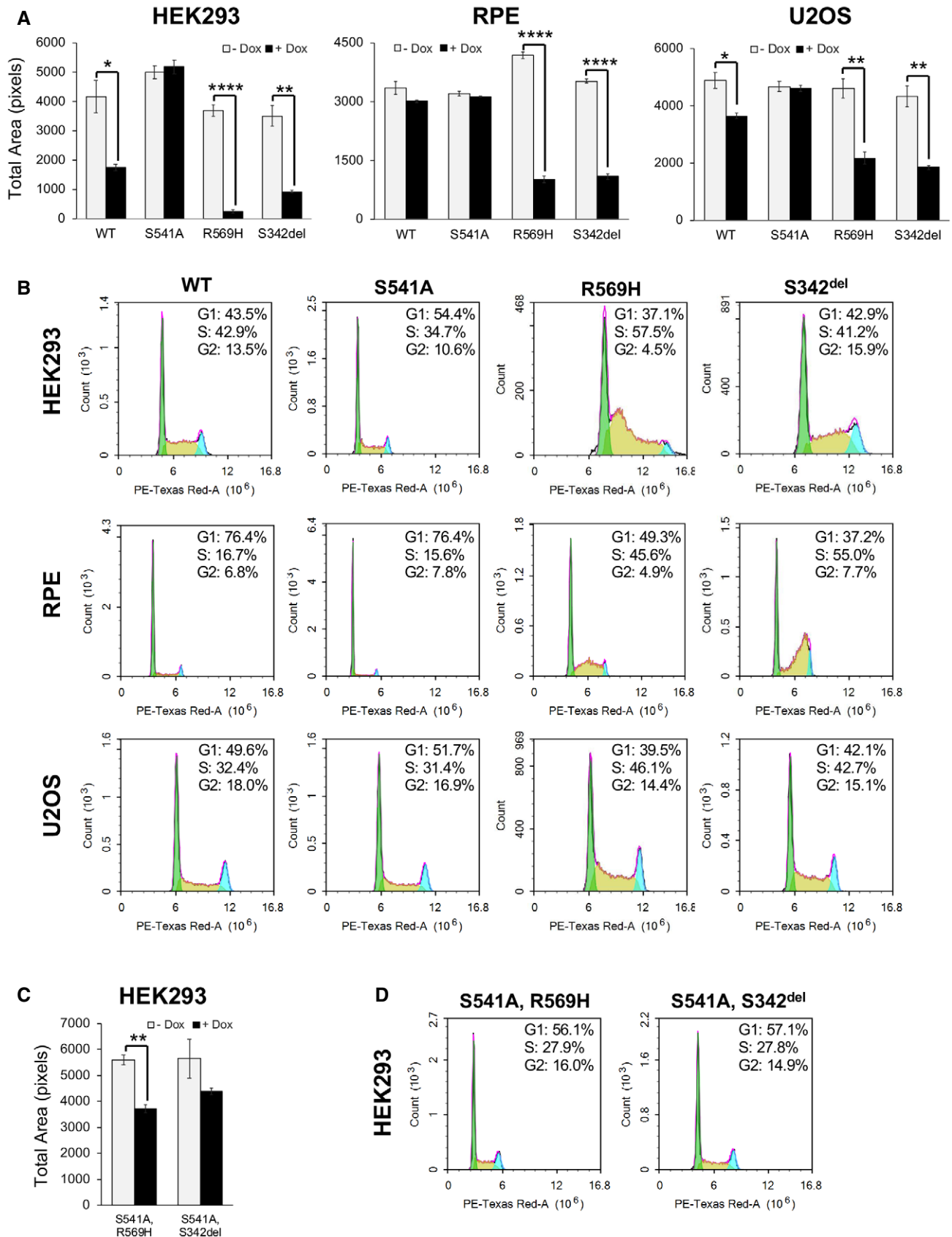
Figure 2.

Figure 2. The effect of overexpressing wild-type or mutant FAM111A on cell growth and cell cycle profiles in multiple cell lines.

A, C HEK293, RPE, or U2OS/MycBioID-FAM111A cell lines were induced with doxycycline to express wild-type or mutant FAM111A for 24 h (HEK293), 48 h (RPE), or 72 h (U2OS). The colonies were fixed then stained with crystal violet. Cell growth was quantitated as total area on ImageJ. Values are mean $\pm$ s.e.m. of independent experiments (*n* = 3). *P < 0.05, **P < 0.01, ****P < 0.0001 (two-tailed unpaired *t*-test).

B, D Cell cycle profiles of HEK293, RPE, and U2OS FAM111A-expressing cell lines that were induced with doxycycline for 48 h and analyzed by flow cytometry.

absent in cells expressing the protease-dead FAM111A constructs (Fig 3B, FAM111A[S541A] and FAM111A[S541A,R569H]). Therefore, the protease activity of FAM111A and FAM111A[R569H] can induce caspase-dependent apoptosis. Notably, however, while Z-VAD-FMK treatment blocked PARP cleavage in both FAM111A and FAM111A[R569H] expressing cells (Fig 3B), it did not reduce the cytotoxicity of FAM111A[R569H] (Fig 3C).

Thus far, our data show that KCS2 and OCS FAM111A patient mutants are gain-of-function and that their elevated protease activity has caspase-independent cytotoxic effects.

BioID-based proteomics identifies candidate targets of FAM111A activity

To define FAM111A protease targets driving the above phenotypes, we used proximity labeling (BioID) of FAM111A and FAM111A[S541A] coupled to mass spectrometry-based protein identification (Roux *et al*, 2012). We reasoned that protease-dead FAM111[S541A] could generate enhanced or more durable biotin labeling of interactors than wild-type, similar to a substrate trap approach.

Candidate FAM111A interactors were identified from both asynchronous and S phase cells (Dataset EV1). Consistent with FAM111A's colocalization with PCNA, several replication-associated proteins were identified including RFC1, RAD18, LIG1, and PCNA (Fig 4A). Despite being proximal to FAM111A, these factors were not consistently enriched in FAM111A[S541A] over wild-type FAM111A purifications, suggesting that they may not be targets of its protease activity.

Interestingly, however, among the most highly enriched proteins identified in FAM111A[S541A] over wild-type FAM111A purifications were a number of nuclear pore complex (NPC) factors (Fig 4A). These included NUP153, POM121, NUP214, NUP50, NUP98, and the multifunctional mRNA export cofactor GANP (Fig 4A and B; Wickramasinghe *et al*, 2010b).

Given our identification of NPC proteins as potential FAM111A targets, we tested the impact of FAM111A hyperactivity on NPC distribution using antibody Mab414, which recognizes several NPC components. Ectopic expression of FAM111A[R569H] caused the nuclei of most cells to "shrivel" and lose their characteristic smooth peripheries, resembling the appearance of early apoptotic nuclei (Fig 4C and Fig EV4A, Mab414). Also, nuclear pores underwent a dramatic redistribution, lost their typical granular appearance, and "clumped" in regions of nuclear invagination or distortion (Fig 4C and Fig EV4A). These phenotypes were not seen upon FAM111A[S541A] overexpression, were dependent on the protease activity of FAM111A[R569H] (see FAM111A[S541A,R569H]), and were consistent across different cell lines (Fig 4C and Fig EV4B). Notably, caspase inhibition again failed to block these FAM111A[R569H]-induced phenotypes (Fig 4C, similar results were obtained with Q-VD-OPH). Therefore, the protease activity of FAM111A[R569H] appears to drive caspase-independent apoptosis-like phenotypes.

In this regard, there have been reports of a caspase-independent change in nuclear structure and barrier function in early apoptosis similar to what we report, which is instead dependent on an unidentified serine protease (Ferrando-May *et al*, 2001; Egger *et al*, 2003; O'Connell & Stenson-Cox, 2007; Strasser *et al*, 2012; Kopeina *et al*, 2018). In the future, it will be interesting to determine if FAM111A is the serine protease in question.

Validating the NPC as a potential target of FAM111A protease activity

GANP is a multifunctional protein whose N-terminus shares homology with the FG repeat-containing nucleoporins (Wickramasinghe *et al*, 2010a). It functions as a scaffold for the TREX-2 mRNA export complex at the NPC (Fischer *et al*, 2002; Wickramasinghe *et al*, 2010b; Bhatia *et al*, 2014), and its C-terminal domain can interact with and acetylate a key replication factor, MCM3 (Kuwahara *et al*, 2000; Takei *et al*, 2001; Takei *et al*, 2002). To validate our FAM111A BioID results, we used a GANP antibody to test its copurification with FAM111A. Western blots revealed the expected enrichment of GANP in FAM111A[S541A] purifications over those of wild-type FAM111A (Fig 4D). As FAM111A overexpression can induce apoptosis-like phenotypes, we tested whether Z-VAD-FMK affects the interaction between wild-type FAM111A and GANP, but found the results were unchanged (Fig 4D). We extended the analysis to include the FAM111A[S541A,R569H] double mutant. Again, GANP was only detected in BioID samples from FAM111A protease-dead mutant expressing cells, including FAM111A[S541A,R569H], indicating that this FAM111A patient mutation does not interfere with GANP interaction (Fig 4E). Thus, protease-dead FAM111A spends longer in proximity to GANP, implying GANP may be proteolyzed by wild-type FAM111A.

Given the dramatic NPC mislocalization caused by FAM111A hyperactivity (Fig 4C), we used the same antibody, Mab414, in Western analysis to detect possible changes in NPC factor abundance. Strikingly, NUP62, the NPC factor most robustly detected by Mab414 in whole cell extracts (Baquero-Perez & Whitehouse, 2015), was strongly depleted upon FAM111A[R569H] expression (Fig 4F). This effect was lessened by ablating the protease activity of FAM111A[R569H] with the additional S541A mutation (Fig 4F, FAM111A[S541A,R569H]). Moreover, NUP62 abundance was lower in cells expressing wild-type FAM111A as compared to those expressing the FAM111[S541A] protease-dead mutant (Fig 4F). Importantly, while Z-VAD-FMK blocked PARP and caspase 3 cleavage, it failed to restore NUP62 levels in cells expressing FAM111A[R569H] (Fig 4F).

NUP62 (p62) is a phenylalanine–glycine (FG) repeat central channel nucleoporin that plays an essential role in gating and transport through the NPC (Rout *et al*, 2003; Lim *et al*, 2007; Tu *et al*, 2013; Chug *et al*, 2015). Although NUP62 was not identified in our FAM111A BioID screen, it localizes within the NPC near NUP153
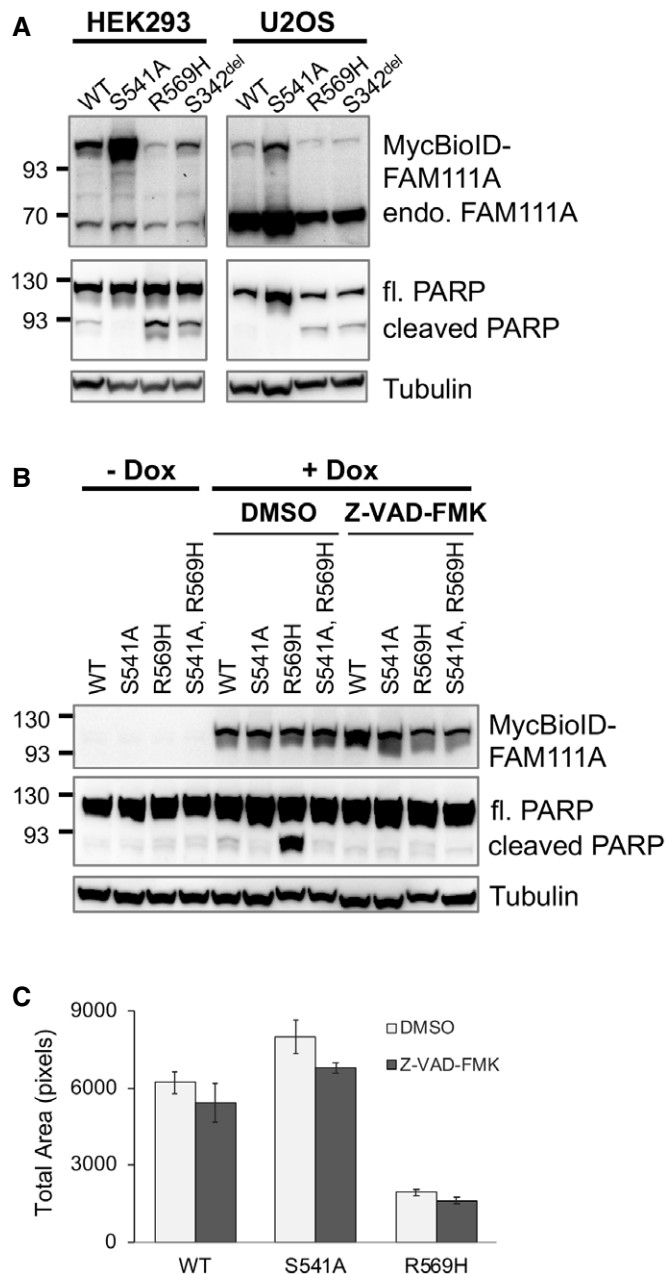
A

B

C

Figure 3. Caspase inhibitor Z-VAD-FMK inhibits PARP cleavage, but not cell death, in cells overexpressing FAM111A[R569H].

A HEK293 or U2OS/MycBioID-FAM111A cell lines were induced with doxycycline for 24 h. Total protein from 10^5 cells was resolved by SDS–PAGE and probed in Western blots for both endogenous FAM111A (71 kDa) and MycBioID-FAM111A (110 kDa) as well as full length and cleaved PARP (116 and 89 kDa, respectively). The Tubulin Western blot is a sample loading control.

B HEK293/MycBioID-FAM111A cell lines with no treatment (- Dox) or treated with doxycycline, along with DMSO or 100 μM Z-VAD-FMK for 24 h (total inhibition of PARP cleavage was also observed when 50 μM Z-VAD-FMK was used). Total protein from ~10^5 cells was resolved by SDS–PAGE and probed in Western blots with Myc, PARP, or Tubulin antibodies.

C HEK293 cell lines were treated with doxycycline and Z-VAD-FMK for 24 h. The colonies were fixed and then stained with crystal violet. Cell growth was quantitated as total area on ImageJ. Values are mean ± s.e.m. of independent experiments ($n = 3$).

and other NPC proteins identified. Such "missed" identifications occur with proximity labeling methods that require spatially available biotinylation sites and also with mass spectrometry-based methods that more readily detect large and abundant proteins. Nevertheless, NUP62 is clearly depleted in a FAM111A-dependent but caspase-independent manner, making it the best candidate target of FAM111A protease activity described to date. NUP62 depletion by FAM111A also fits well with FAM111A's induction of nuclear permeability during viral replication, as shown below. Whether NUP62 depletion contributes to KCS2/OCS development requires further study. However, it is interesting that clinically overlapping KCS1 is caused by mutations in a tubulin cofactor, TBCE (Parvari et al, 2002). Therefore, future studies on the etiology of KCS2/OCS should not only focus on the DNA replication defects caused by FAM111A hyperactivity.

FAM111A induces changes in nuclear permeability during viral replication

FAM111A is an SV40 HR restriction factor, which interacts with and is likely inactivated by the C-terminus of wild-type SV40 large T antigen (LT; (Fine et al, 2012)). That is, FAM111A antagonizes the formation of replication centers of SV40 HR mutants that contain LT C-terminal mutations e.g. SV40[HR684] (Tarnita et al, 2019). FAM111A also restricts an orthopoxvirus HR mutant that lacks the serpin family serine protease inhibitor SPI-1, suggesting it has broad antiviral activity (Panda et al, 2017). Despite these advances, how FAM111A restricts viral challenges remains poorly defined.

Our results show that FAM111A activity can impair cellular viability and induce apoptosis-like phenotypes. However, the data so far are most relevant to the situation in KCS2 or OCS patients, where FAM111A is hyperactive (Unger et al, 2013). We therefore tested the impact of endogenous wild-type FAM111A on cells when challenged by SV40. To this end, we transfected U2OS cells with wild-type SV40 or two HR mutants SV40[HR684] and SV40[dl1066] (Poulin & DeCaprio, 2006; Tarnita et al, 2019).

Indirect immunofluorescence (IF) analysis of wild-type SV40 LT revealed a consistently nuclear localization in U2OS cells over the 72-h time course, as reported previously (Figs 5A and B, and Fig EV5A; (Tarnita et al, 2019)). In contrast, the SV40[HR684] and SV40[dl1066] HR mutants developed a progressively more pan-cellular LT distribution, after an initial nuclear localization at 24 h (Figs 5A and B, and Fig EV5A). In addition, the nuclei of cells transfected with SV40[HR684] appeared to partially shrivel and nucleoporins underwent a dramatic redistribution (Fig EV5B), as seen with FAM111A[R569H] overexpression.

To test whether SV40[HR684] and SV40[dl1066] transfected cells actually lose normal nuclear barrier function, we co-expressed an independent 2XRFP-NLS nuclear reporter (Hatch et al, 2013). The loss of reporter compartmentalization mirrored that of the SV40 HR LT mutants (Fig 5C). Therefore, rather than a specific defect in the nuclear retention of LT HR mutants, nuclear barrier function is generally compromised. Importantly, depletion of FAM111A rescued the above phenotypes, including increased nuclear permeability (Fig 5A–C). Therefore, the wild-type, but not SV40[HR684] and SV40[dl1066], LT antagonizes FAM111A activity, which otherwise causes nuclear dysfunction.

We next analyzed LT levels by Western blot, as they reflect the ability of SV40 to transcribe and replicate its genome. As previously
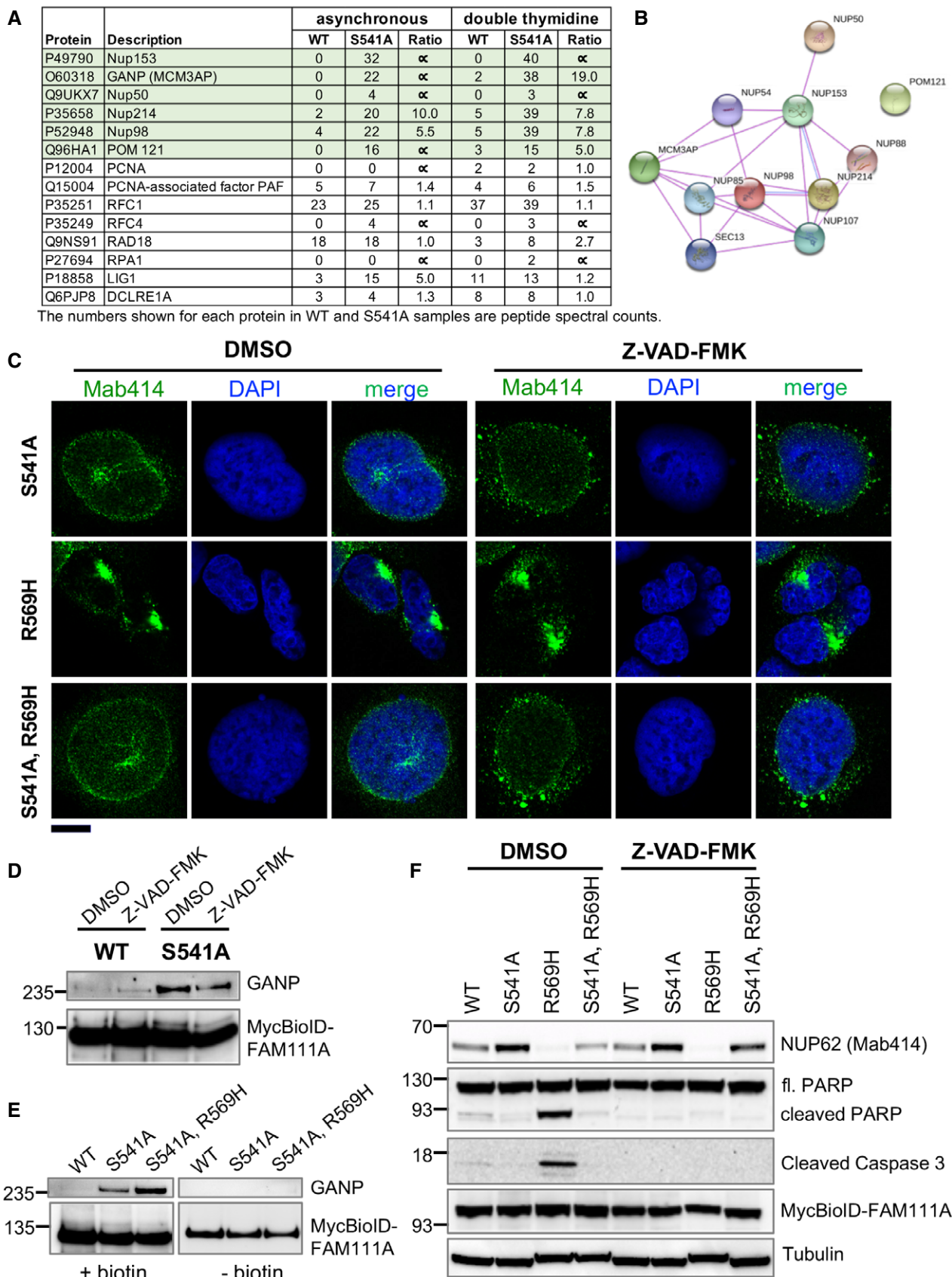
A

Protein	Description	asynchronous			double thymidine		
		WT	S541A	Ratio	WT	S541A	Ratio
P49790	Nup153	0	32	∝	0	40	∝
O60318	GANP (MCM3AP)	0	22	∝	2	38	19.0
Q9UKX7	Nup50	0	4	∝	0	3	∝
P35658	Nup214	2	20	10.0	5	39	7.8
P52948	Nup98	4	22	5.5	5	39	7.8
Q96HA1	POM 121	0	16	∝	3	15	5.0
P12004	PCNA	0	0	∝	2	2	1.0
Q15004	PCNA-associated factor PAF	5	7	1.4	4	6	1.5
P35251	RFC1	23	25	1.1	37	39	1.1
P35249	RFC4	0	4	∝	0	3	∝
Q9NS91	RAD18	18	18	1.0	3	8	2.7
P27694	RPA1	0	0	∝	0	2	∝
P18858	LIG1	3	15	5.0	11	13	1.2
Q6PJP8	DCLRE1A	3	4	1.3	8	8	1.0

The numbers shown for each protein in WT and S541A samples are peptide spectral counts.

B

C

D

E

F

Figure 4.

reported, wild-type SV40 LT expression peaked at 48 h and sustained through 72 h, whereas SV40^{HR684} and SV40^{dl1066} LT expression was weaker overall and tapered off by 72 h (Fig 5D; (Tarnita *et al*, 2019)). Interestingly, PARP cleavage was higher in SV40^{HR684} and SV40^{dl1066} than wild-type SV40 transfected cells, being strongest at 72 h when loss of nuclear barrier function peaks for the HR mutants (Fig 5D). Importantly, FAM111A depletion largely suppressed the differences in LT expression profiles of wild-type and HR mutant SV40 and reduced PARP cleavage in SV40^{HR684} and SV40^{dl1066} cells (Fig 5D).

FAM111A appears to execute its restrictive function during viral DNA replication (Panda *et al*, 2017; Tarnita *et al*, 2019), which fits with its localization to cellular DNA replication sites and the negative effects of FAM111A^{R569H} on processive replication. To determine whether SV40 replication triggers the FAM111A-dependent loss of nuclear barrier function, we used an LT mutation (D474N) that abolishes its helicase activity and SV40 genome replication (Huang *et al*, 2010).

We generated the single SV40^{D474N} LT mutant and the double SV40^{D474N,HR684} LT mutant for analysis by IF and Western blot. SV40^{D474N} LT was almost exclusively nuclear at all time points, and Western analysis revealed a wild-type expression profile that did not taper at 72 h (Fig 5A–D). Importantly, the SV40^{D474N,HR684} double mutant behaved like the SV40^{D474N} single mutant in terms of nuclear localization and expression profile (Fig 5A–D). In addition, unlike the SV40^{HR684} LT, FAM111A depletion had no impact on the expression profile of SV40^{D474N} or SV40^{D474N,HR684} LT (Fig 5A–D). Thus, it is not simply SV40^{HR684} LT expression that causes nuclear permeability changes, rather; it is SV40 replication in the presence of FAM111A activity.

Given that hyperactive FAM111A^{R569H} disrupts cellular DNA replication, we envisioned that FAM111A could directly inhibit viral replication by degrading key replication factors. Crucially however, although others and we have identified replication factors as FAM111A interactors, to date none appear to be targets of its protease activity (Hoffmann *et al*, 2020). Instead, FAM111A causes nuclear barrier dysfunction, among other phenotypes, when SV40 HR mutants attempt to replicate in restrictive cells. These effects, which are strikingly similar to those caused by the KCS2 and OCS FAM111A patient mutants, could *indirectly* inhibit both viral and cellular DNA replication.

We do not believe that the induction of apoptosis is a primary restrictive function of FAM111A. Instead, FAM111A triggers early nuclear barrier dysfunction in the absence of late apoptotic phenotypes. As mentioned above, an unidentified serine protease was implicated in the caspase-independent loss of nuclear barrier

function in response to different types of cell stress (Ferrando-May *et al*, 2001; Egger *et al*, 2003; O'Connell & Stenson-Cox, 2007; Strasser *et al*, 2012; Kopeina *et al*, 2018). In addition, early studies revealed that RPXV and VACV HR mutants that lack the serine protease inhibitor SPI-1 cause alterations in the nuclear morphology of restrictive cells (Brooks *et al*, 1995; Shisler *et al*, 1999). Together with the fact that FAM111A is a restriction factor for VACV SPI-1Δ (Panda *et al*, 2017), our data suggest that the disruption of cell function by nuclear barrier loss could be a common function for FAM111A in restricting viral replication.

Together, our results demonstrate that FAM111A exhibits protease-dependent cytotoxicity, which is amplified by the KCS2 and OCS patient mutants, consistent with recent studies (Kojima *et al*, 2020; Hoffmann *et al*, 2020). Thus, FAM111A hyperactivity can explain the dominant effects of FAM111A^{R569H} and FAM111A^{S342del} over wild-type in the heterozygous disease state (Unger *et al*, 2013). Moreover, we show that hyperactive FAM111A compromises nuclear barrier function, S phase progression, and cell viability, possibly in part through the proteolysis of the NPC factors GANP and NUP62. Such effects could negatively impact parathyroid development (among other systems) causing KCS2 and OCS phenotypes (Unger *et al*, 2013). These same effects could also prevent SV40 HR mutant replication in restrictive cells.

Consistent with its S phase localization, FAM111A is in close proximity to DNA replication factors such as RFC1 and PCNA, but these do not appear to be targets of FAM111A protease activity (see also Hoffmann *et al*, 2020). Instead, FAM111A likely cooperates with PCNA and RFC1-5 at both cellular and viral genome replication sites. Indeed, FAM111A appears to remove cellular replication fork-blocking DNA-protein complexes, e.g., TOP1cc, and collaborates with RFC1-5 to restrict the replication of HR mutant poxviruses (Panda *et al*, 2017; Kojima *et al*, 2020). Therefore, FAM111A may be "activated" at replication forks to promote replication fork progression, and depending on the context, degrade NPC or other factors to control cell function.

At a glance, FAM111A's localization to replication forks and its targeting of the NPC seem incompatible. Interestingly, however, nucleoporins and GANP make chromatin contacts to spatially organize chromatin, control its outputs such as transcription, and maintain genome stability (Ibarra & Hetzer, 2015). Moreover, when FAM111A is at the replication fork, several nucleoporins and GANP are actually *depleted* from nascent chromatin (Alabert *et al*, 2014; Wessel *et al*, 2019). Therefore, we speculate that FAM111A could help displace nuclear pore-chromatin interactions to facilitate replication fork progression, as seen at actively transcribed genes (Brickner & Brickner, 2011).
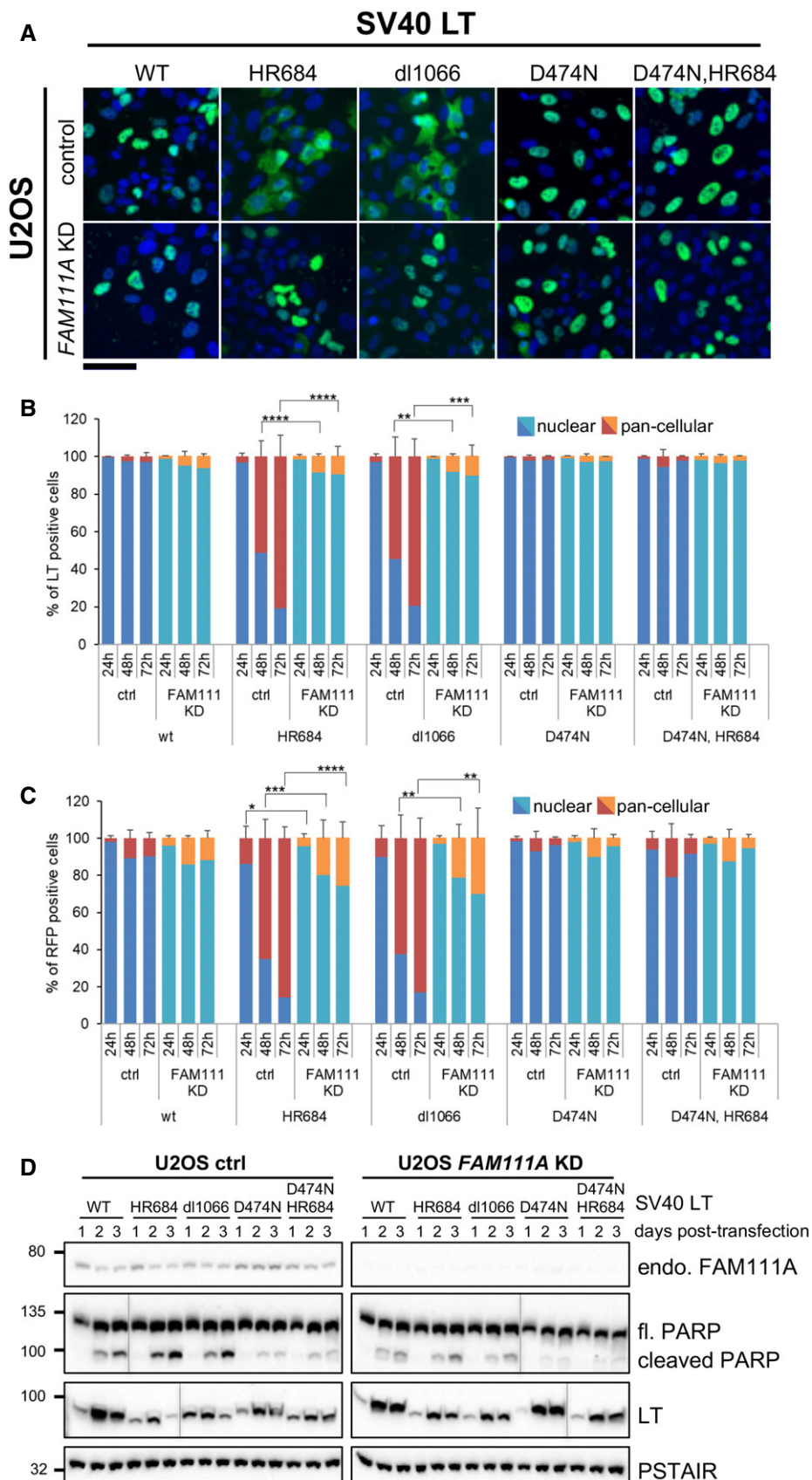
Figure 5.

Overall, we propose a model in which the loading of PCNA by RFC1-5 acts as a DNA sensor that recruits FAM111A to endogenous replication sites or viral genomes that utilize/attract PCNA (Sowd & Fanning, 2012; Postigo *et al*, 2017). During unscheduled viral DNA replication or in KCS2/OCS patients, FAM111A is hyperactivated and cytotoxic due to the absence of normal protease regulation. Wild-type SV40 LT and VACV SPI-1 are able to inhibit FAM111A, preventing both local protease activity (at viral replication centers) and nuclear barrier dysfunction, thereby enabling viral replication. In the future, it will be interesting to define endogenous regulatory mechanisms for FAM111A, and if its protease activity can be therapeutically targeted.

Materials and Methods

Cell culture

Human embryonic kidney cell lines HEK293 and HEK293T, human osteosarcoma cell line U2OS, human colon cancer line HCT116, and human cervical adenocarcinoma cell line HeLa were obtained from American Type Culture Collection (ATCC). Human epithelial cells immortalized with hTERT cell line RPE was obtained from Denchi lab (Loe *et al*, 2020). These cell lines were cultured in Dulbecco's modified Eagle's medium (DMEM) supplemented with 10% fetal bovine serum (FBS).

Unless otherwise indicated, the following drug concentrations were used: doxycycline (1 μg/ml, Sigma-Aldrich), biotin (50 μM, Sigma-Aldrich, B4501), and Z-VAD-FMK (50 or 100 μM, APExBIO, A1902).

Plasmids

Full-length human *FAM111A* cDNA was PCR-amplified and inserted into destination vectors using In-Fusion seamless cloning (Takara Bio). The pTRIPz-MycBioID vector allows for doxycycline-inducible expression of FAM111A with N-terminal fusion of a Myc tag and a promiscuous biotin ligase (MycBioID; Roux *et al*, 2012). Point mutations in FAM111A and SV40 large T antigen (LT) were introduced using the QuikChange Site-Directed Mutagenesis kit (Agilent Technologies) according to the manufacturer's protocol. All cloning and mutagenesis were verified by sequencing. Plasmids and stable cell lines used in this study are listed in supplemental tables (Tables EV1 and EV2).

RNAi

Stable RNAi was achieved by viral shRNA generated in pLKO.1-blast (Bryant *et al*, 2010). Knockdown was verified by standard Western blot,

normalizing to Tubulin or Cdc2 expression. pLKO.1 lentiviruses were constructed according to the Addgene pLKO.1 protocol (www.addgene.org), with target sequences found in Mission shRNA database (Sigma-Aldrich). RNAi target sequences used in this research include:

Control-sh: 5'-CCTAAGGTTAAGTCGCCCTCG-3'.
FAM111A-sh1: 5'-GTCAATGTGTAAGGGTGACAT-3'.

Transfection, virus production, and transduction

For lentivirus production, pTRIPz or pLKO.1 plasmid was cotransfected with lentiviral packaging vectors (pMD2.G and psPAX2) into HEK293T using TransIT-LT1 (Mirus) transfection reagent following the manufacturer instruction. All supernatants were passed through 0.45-μm filters to remove cell debris. The supernatants were either immediately applied to the target cells or frozen in liquid nitrogen for further use. For lentivirus transduction (pLKO.1, pTRIPz), subconfluent U2OS, RPE, HEK293, or 293T cultures were infected with virus-containing supernatants for 12–16 h at 37°C. Viral supernatants were then replaced with fresh growth medium and cultured for a further 72 h with appropriate antibiotic selection. Puromycin (0.5 μg/ml for U2OS; 2 μg/ml for HEK293, 293T) and blasticidin (12 μg/ml) were used. To generate stable cell lines (Table EV2), the transduced cells were cultured in the presence of antibiotic selection until all control cells were killed. SV40 plasmid transfections were conducted using TransIT LT1 (Mirus) transfection reagent following the manufacturer's instructions.

Immunofluorescence and microscopy

The cells grown on coverslips were fixed in 4% formaldehyde in PBS for 10 min and then permeabilized with PBS containing 0.2% Triton X-100 for 5 min at room temperature. The cells stained for PCNA were pre-extracted in Triton X-100 buffer containing 0.5% Triton X-100, 20 mM HEPES (pH 7.9), 50 mM NaCl, 3 mM $MgCl_2$, and 300 mM Sucrose for 2 min on ice and then fixed in 3% formaldehyde and 2% sucrose in PBS for 10 min at room temperature. The cells were incubated with primary antibodies diluted in blocking solution of 5% Normal Goat Serum (BioLegend, 927502) or 0.2% (w/v) cold water fish gelatin (Sigma, G-7765) and 0.5% (w/v) BSA (Sigma, A-2153) in PBS for 1 h at room temperature or at 4°C overnight. Following staining with secondary antibodies and 0.1 μg/ml 4',6-diamidino-2-phenylindole dihydrochloride (DAPI, Sigma, D-9542) diluted in 5% NGS-PBS, cells were mounted onto glass slides using ProLong Gold Antifade (Invitrogen, #P36934). Primary antibodies used for immunofluorescence included: FAM111A (Abcam, ab184572; 1:100), SV40LT (Abcam, ab16879; 1:250), PCNA (Santa Cruz, sc-56; 1:200), PML (Santa Cruz, sc-966; 1:200), and anti-Nuclear Pore Complex proteins (Mab414, Abcam,

ab24609; 1:200). Secondary antibodies used were Alexa Fluor Secondary Antibodies (Life Technologies).

Confocal images were acquired with a Zeiss LSM 880 inverted spectral imaging confocal microscope (Carl Zeiss Microscopy) equipped with 63x/1.4 oil immersion high NA objective lens, using standard settings in Zen microscope software. Data were exported and processed using ImageJ software (NIH). Digital images were also taken using Zeiss Axio Imager M1 with 20x and 60x oil immersion objectives.

Clonogenic survival assays

Cells were counted and seeded in six-well plates (seven hundred fifty cells for U2OS, five hundred cells for other cell lines), allowed to adhere overnight. The next day, 1 μg/ml of doxycycline was added to the media. Twenty-four (HEK293, 293T), forty-eight (RPE), or seventy-two (U2OS) hours later, doxycycline was removed, and fresh medium was added. Cells were cultured for another four to five days until visible colonies have formed. Subsequently, the cells were fixed with 10% neutral-buffered formalin and stained with 0.5% crystal violet. The plates were scanned on LI-COR (LI-COR Biosciences). Cell growth was quantitated as total area using ImageJ software (NIH).

Flow cytometry

For analysis of DNA content, cells were fixed with ice-cold 70% EtOH, stained with 10 μg/ml propidium iodide, and treated with 100 μg/ml RNase A in PBS containing 0.1% Triton X-100. Flow cytometry analysis was performed on a NovoCyte 3000 Flow Cytometer (ACEA Biosciences) using NovoExpress software.

BioID labeling and affinity purification of biotinylated proteins

Cells were incubated for 24 h in complete media supplemented with doxycycline and biotin. After washing with PBS, cells ($2-5 \times 10^6$ cells for small-scale analysis; 2×10^7 cells for large scale analysis) were collected and frozen. Cell pellets were lysed and processed as described (Roux *et al*, 2012). Briefly, each 10^6 cells were suspended in 100 μl of strong lysis buffer containing 50 mM Tris, pH 7.5, 500 mM NaCl, 0.4% SDS, 5 mM EDTA, 1 mM DTT, 1× Halt Protease Inhibitor Cocktail (Thermo Fisher, 78430), and 1 mM PMSF. The lysate was sonicated in a Misonix waterbath Sonicator. Triton X-100 was added to 2% final concentration, and sonication was repeated. Equal volume of cold 50 mM Tris, pH 7.4 was added, followed by additional sonication. After centrifugation at 16,000 *g* for 10 min at 4°C, supernatants were incubated with Dynabeads MyOne Streptavidin C1 (Thermo Fisher, 65002) at 4°C for 2 h (20 μl of beads were used for small-scale analysis; 100 μl for large scale preparation for mass spectrometry). Following incubation, the beads were washed at 25°C sequentially in 1 ml of 2% SDS (wash buffer 1) twice, once each in 0.1% deoxycholate, 1% Triton X-100, 500 mM NaCl, 1 mM EDTA, and 50 mM HEPES, pH 7.5 (wash buffer 2), in 250 mM LiCl, 0.5% NP-40, 0.5% deoxycholate, 1 mM EDTA, and 10 mM Tris, pH 8.1 (wash buffer 3), and finally twice in 50 mM Tris, pH 7.4, 50 mM NaCl (wash buffer 4). For Western blot analysis, proteins were eluted from the magnetic beads with 35 μl of 2× NuPAGE LDS Sample Loading Buffer (Thermo Fisher,

NP0007) with 100 mM DTT at 100°C for 5 min. For mass spectrometry analysis, the beads were washed and stored in 100 ml of 8 M urea, 100 mM Tris, pH 8.5, until further processing.

Western blotting

Cells were lysed in strong lysis buffer described in the section above. The whole cell lysate was combined with NuPAGE LDS Sample Loading Buffer and 100 mM DTT, separated by SDS–PAGE and transferred to nitrocellulose. Immunoblotting was performed as described (Nie *et al*, 2017). Antibodies used for immunoblotting included: cleaved Caspase-3 (Asp175) (Cell Signaling, #9661; 1:1,000), FAM111A (Abcam, ab184572; 1:1,000), Myc 9E10 (Scripps Antibody Core Facility; 1:3,000), PARP (Cell Signaling, 9542; 1:1,000), anti-Nuclear Pore Complex proteins (Mab414, Abcam, ab24609; 1:1,000), GANP (Bethyl, A303-128A; 1:1,000), SV40LT (Abcam, ab16879; 1:3,000), tubulin alpha (Sigma, T9026; 1:10,000), and Cdc2-PSTAIR (Abcam, ab10345; 1:15,000). Following incubation with HRP-conjugated secondary antibodies, proteins were detected with SuperSignal West Dura Extended Duration Substrate (Thermo Fisher, 34076) on the ChemiDox XRS + System (BioRad).

Protein identification by mass spectrometry

Protein samples were reduced and alkylated by sequential incubation with 5 mM Tris (2-carboxyethyl) phosphine for 20 min at room temperature and 10 mM iodoacetamide reagent in the dark at room temperature for 20 additional min. Proteins were digested sequentially at 37°C with lys-C for 4 h followed by trypsin for 12 h. After quenching the digest by the addition of formic acid to 5% (v/v), peptides were desalted using Pierce C18 tips (Thermo Fisher Scientific), dried by vacuum centrifugation, and resuspended in 5% formic acid. Peptides were fractionated online using reversed phase chromatography on in-house packed C18 columns. The 140-min gradient of increasing acetonitrile was delivered using a Dionex Ultimate 3000 UHPLC system (Thermo Fisher Scientific). Peptides were electrosprayed into the mass spectrometer by the application of a distal *2.2* kV spray voltage. MS/MS data were acquired using an Orbitrap Fusion Lumos mass spectrometer operating in Data-Dependent Acquisition (DDA) mode consisting of a full MS1 scan to identify peptide precursors that were subsequently targeted by MS2 scans (Resolution = 15,000) using high energy collision dissociation for the remainder of the 3 s cycle time. Data analysis was performed using the Integrated Proteomics bioinformatic pipeline 2 (Integrated Proteomics Applications, San Diego, CA). Database searching was performed using the ProLuCID algorithm against the EMBL Human reference proteome (UP000005640 9606). Peptides identifications were filtered using a 1% FDR as estimated using a decoy database. Proteins were considered present in a sample if they had 2 or more unique peptides mapping to them. Relative comparisons between samples to identify candidate FAM111A interacting proteins were done using raw peptide spectral counts.

Data availability

The datasets produced in this study are available in the PRIDE database (Perez-Riverol *et al*, 2019) as detailed below: Protein

interaction AP-MS data: PRIDE PXD020327 (http://www.ebi.ac.uk/pride/archive/projects/PXD020327).

Expanded View for this article is available online.

Author contributions
MNB, MN, MO, EL-D, YJ-A, and JAW devised and executed experiments in support of the study. MN and MO performed most of the presented experiments. YJ-A and JAW carried out mass spectrometry-based protein identification analysis of our FAM111A BioID samples. All authors contributed to manuscript writing and figure preparation.

Conflict of interest
The authors declare that they have no conflict of interest.

References

Alabert C, Bukowski-Wills J-C, Lee S-B, Kustatscher G, Nakamura K, de Lima Alves F, Menard P, Mejlvang J, Rappsilber J, Groth A (2014) Nascent chromatin capture proteomics determines chromatin dynamics during DNA replication and identifies unknown fork components. *Nat Cell Biol* 16: 281–293

Baquero-Perez B, Whitehouse A (2015) Hsp70 isoforms are essential for the formation of Kaposi's sarcoma-associated herpesvirus replication and transcription compartments. *PLoS Pathog* 11: e1005274

Bhatia V, Barroso SI, Garcia-Rubio ML, Tumini E, Herrera-Moyano E, Aguilera A (2014) BRCA2 prevents R-loop accumulation and associates with TREX-2 mRNA export factor PCID2. *Nature* 511: 362–365

Brickner DG, Brickner JH (2011) Gene positioning is regulated by phosphorylation of the nuclear pore complex by Cdk1. *Cell Cycle* 10: 392–395

Brooks MA, Ali AN, Turner PC, Moyer RW (1995) A rabbitpox virus serpin gene controls host range by inhibiting apoptosis in restrictive cells. *J Virol* 69: 7688–7698

Bryan TM, Englezou A, Dallapozza L, Dunham MA, Reddel RR (1997) Evidence for an alternative mechanism for maintaining telomere length in human tumors and tumor-derived cell lines. *Nat Med* 3: 1271–1274

Bryant DM, Datta A, Rodriguez-Fraticelli AE, Peranen J, Martin-Belmonte F, Mostov KE (2010) A molecular network for de novo generation of the apical surface and lumen. *Nat Cell Biol* 12: 1035–1045

Cesare AJ, Reddel RR (2010) Alternative lengthening of telomeres: models, mechanisms and implications. *Nat Rev Genet* 11: 319–330

Chug H, Trakhanov S, Hulsmann BB, Pleiner T, Gorlich D (2015) Crystal structure of the metazoan Nup62*Nup58*Nup54 nucleoporin complex. *Science* 350: 106–110

Dilley RL, Verma P, Cho NW, Winters HD, Wondisford AR, Greenberg RA (2016) Break-induced telomere synthesis underlies alternative telomere maintenance. *Nature* 539: 54–58

Egger L, Schneider J, Rheme C, Tapernoux M, Hacki J, Borner C (2003) Serine proteases mediate apoptosis-like cell death and phagocytosis under caspase-inhibiting conditions. *Cell Death Differ* 10: 1188–1203

Ferrando-May E, Cordes V, Biller-Ckovric I, Mirkovic J, Gorlich D, Nicotera P (2001) Caspases mediate nucleoporin cleavage, but not early redistribution of nuclear transport factors and modulation of nuclear permeability in apoptosis. *Cell Death Differ* 8: 495–505

Fine DA, Rozenblatt-Rosen O, Padi M, Korkhin A, James RL, Adelmant G, Yoon R, Guo L, Berrios C, Zhang Y *et al* (2012) Identification of FAM111A as an SV40 host range restriction and adenovirus helper factor. *PLoS Pathog* 8: e1002949

Fischer T, Strasser K, Racz A, Rodriguez-Navarro S, Oppizzi M, Ihrig P, Lechner J, Hurt E (2002) The mRNA export machinery requires the novel Sac3p-Thp1p complex to dock at the nucleoplasmic entrance of the nuclear pores. *EMBO J* 21: 5843–5852

Hatch EM, Fischer AH, Deerinck TJ, Hetzer MW (2013) Catastrophic nuclear envelope collapse in cancer cell micronuclei. *Cell* 154: 47–60

Hoffmann S, Pentakota S, Mund A, Haahr P, Coscia F, Gallo M, Mann M, Taylor NM, Mailand N (2020) FAM111 protease activity undermines cellular fitness and is amplified by gain-of-function mutations in human disease. *EMBO Rep* 21, e50662

Huang H, Zhao K, Arnett DR, Fanning E (2010) A specific docking site for DNA polymerase {alpha}-primase on the SV40 helicase is required for viral primosome activity, but helicase activity is dispensable. *J Biol Chem* 285: 33475–33484

Ibarra A, Hetzer MW (2015) Nuclear pore proteins and the control of genome functions. *Genes Dev* 29: 337–349

Isojima T, Doi K, Mitsui J, Oda Y, Tokuhiro E, Yasoda A, Yorifuji T, Horikawa R, Yoshimura J, Ishiura H *et al* (2014) A recurrent de novo FAM111A mutation causes Kenny-Caffey syndrome type 2. *J Bone Miner Res* 29: 992–998

Kojima Y, Machida Y, Palani S, Caulfield TR, Radisky ES, Kaufmann SH, Machida YJ (2020) FAM111A protects replication forks from protein obstacles via its trypsin-like domain. *Nat Commun* 11: 1318

Kopeina GS, Prokhorova EA, Lavrik IN, Zhivotovsky B (2018) Alterations in the nucleocytoplasmic transport in apoptosis: caspases lead the way. *Cell Prolif* 51: e12467

Kuwahara K, Yoshida M, Kondo E, Sakata A, Watanabe Y, Abe E, Kouno Y, Tomiyasu S, Fujimura S, Tokuhisa T *et al* (2000) A novel nuclear phosphoprotein, GANP, is up-regulated in centrocytes of the germinal center and associated with MCM3, a protein essential for DNA replication. *Blood* 95: 2321–2328

Lim RY, Fahrenkrog B, Koser J, Schwarz-Herion K, Deng J, Aebi U (2007) Nanomechanical basis of selective gating by the nuclear pore complex. *Science* 318: 640–643

Loe TK, Li JSZ, Zhang Y, Azeroglu B, Boddy MN, Denchi EL (2020) Telomere length heterogeneity in ALT cells is maintained by PML-dependent localization of the BTR complex to telomeres. *Genes Dev* 34: 650–662

Luttge BG, Moyer RW (2005) Suppressors of a host range mutation in the rabbitpox virus serpin SPI-1 map to proteins essential for viral DNA replication. *J Virol* 79: 9168–9179

Min J, Wright WE, Shay JW (2017) Alternative lengthening of telomeres can be maintained by preferential elongation of lagging strands. *Nucleic Acids Res* 45: 2615–2628

Nie M, Moser BA, Nakamura TM, Boddy MN (2017) SUMO-targeted ubiquitin ligase activity can either suppress or promote genome instability, depending on the nature of the DNA lesion. *PLoS Genet* 13: e1006776

Nikkel SM, Ahmed A, Smith A, Marcadier J, Bulman DE, Boycott KM (2014) Mother-to-daughter transmission of Kenny-Caffey syndrome associated

with the recurrent, dominant FAM111A mutation p.Arg569His. *Clin Genet* 86: 394 – 395

O'Connell AR, Stenson-Cox C (2007) A more serine way to die: defining the characteristics of serine protease-mediated cell death cascades. *Biochim Biophys Acta* 1773: 1491 – 1499

Pan X, Drosopoulos WC, Sethi L, Madireddy A, Schildkraut CL, Zhang D (2017) FANCM, BRCA1, and BLM cooperatively resolve the replication stress at the ALT telomeres. *Proc Natl Acad Sci USA* 114: E5940 – E5949

Panda D, Fernandez DJ, Lal M, Buehler E, Moss B (2017) Triad of human cellular proteins, IRF2, FAM111A, and RFC3, restrict replication of orthopoxvirus SPI-1 host-range mutants. *Proc Natl Acad Sci USA* 114: 3720 – 3725

Parvari R, Hershkovitz E, Grossman N, Gorodischer R, Loeys B, Zecic A, Mortier G, Gregory S, Sharony R, Kambouris M *et al* (2002) Mutation of TBCE causes hypoparathyroidism-retardation-dysmorphism and autosomal recessive Kenny-Caffey syndrome. *Nat Genet* 32: 448 – 452

Perez-Riverol Y, Csordas A, Bai J, Bernal-Llinares M, Hewapathirana S, Kundu DJ, Inuganti A, Griss J, Mayer G, Eisenacher M *et al* (2019) The PRIDE database and related tools and resources in 2019: improving support for quantification data. *Nucleic Acids Res* 47: D442 – D450

Postigo A, Ramsden AE, Howell M, Way M (2017) Cytoplasmic ATR activation promotes vaccinia virus genome replication. *Cell Rep* 19: 1022 – 1032

Poulin DL, Decaprio JA (2006) The carboxyl-terminal domain of large T antigen rescues SV40 host range activity in trans independent of acetylation. *Virology* 349: 212 – 221

Rout MP, Aitchison JD, Magnasco MO, Chait BT (2003) Virtual gating and nuclear transport: the hole picture. *Trends Cell Biol* 13: 622 – 628

Roux KJ, Kim DI, Raida M, Burke B (2012) A promiscuous biotin ligase fusion protein identifies proximal and interacting proteins in mammalian cells. *J Cell Biol* 196: 801 – 810

Shisler JL, Isaacs SN, Moss B (1999) Vaccinia virus serpin-1 deletion mutant exhibits a host range defect characterized by low levels of intermediate and late mRNAs. *Virology* 262: 298 – 311

Sobinoff AP, Pickett HA (2020) Mechanisms that drive telomere maintenance and recombination in human cancers. *Curr Opin Genet Dev* 60: 25 – 30

Soldani C, Scovassi AI (2002) Poly(ADP-ribose) polymerase-1 cleavage during apoptosis: an update. *Apoptosis* 7: 321 – 328

Sowd GA, Fanning E (2012) A wolf in sheep's clothing: SV40 co-opts host genome maintenance proteins to replicate viral DNA. *PLoS Pathog* 8: e1002994

Strasser C, Grote P, Schauble K, Ganz M, Ferrando-May E (2012) Regulation of nuclear envelope permeability in cell death and survival. *Nucleus* 3: 540 – 551

Takei Y, Assenberg M, Tsujimoto G, Laskey R (2002) The MCM3 acetylase MCM3AP inhibits initiation, but not elongation, of DNA replication via interaction with MCM3. *J Biol Chem* 277: 43121 – 43125

Takei Y, Swietlik M, Tanoue A, Tsujimoto G, Kouzarides T, Laskey R (2001) MCM3AP, a novel acetyltransferase that acetylates replication protein MCM3. *EMBO Rep* 2: 119 – 123

Tarnita RM, Wilkie AR, Decaprio JA (2019) Contribution of DNA replication to the FAM111A-mediated simian virus 40 host range phenotype. *J Virol* 93: e01330-18

Tu LC, Fu G, Zilman A, Musser SM (2013) Large cargo transport by nuclear pores: implications for the spatial organization of FG-nucleoporins. *EMBO J* 32: 3220 – 3230

Unger S, Gorna MW, le Bechec A, Do Vale-Pereira S, Bedeschi MF, Geiberger S, Grigelioniene G, Horemuzova E, Lalatta F, Lausch E *et al* (2013) FAM111A mutations result in hypoparathyroidism and impaired skeletal development. *Am J Hum Genet* 92: 990 – 995

Wessel SR, Mohni KN, Luzwick JW, Dungrawala H, Cortez D (2019) Functional analysis of the replication fork proteome identifies BET proteins as PCNA regulators. *Cell Rep* 28: 3497 – 3509

Wickramasinghe VO, McMurtrie PI, Mills AD, Takei Y, Penrhyn-Lowe S, Amagase Y, Main S, Marr J, Stewart M, Laskey RA (2010a) mRNA export from mammalian cell nuclei is dependent on GANP. *Curr Biol* 20: 25 – 31

Wickramasinghe VO, Stewart M, Laskey RA (2010b) GANP enhances the efficiency of mRNA nuclear export in mammalian cells. *Nucleus* 1: 393 – 396

Zhang JM, Yadav T, Ouyang J, Lan L, Zou L (2019) Alternative lengthening of telomeres through two distinct break-induced replication pathways. *Cell Rep* 26: 955 – 968